Modifications of Nuclear Architecture and Chromatin Organization in Ataxia Telangiectasia Cells Are Coupled to Changes of Gene Transcription

Myriam Grattarola,[1] Cristina Borghi,[2] Laura Emionite,[3] Patrizia Lulli,[4] Luciana Chessa,[4] and Laura Vergani[1]*

[1]Department of Biophysical Sciences and Techologies M.&O.-Biophysical Division, University of Genova, Genova, Italy
[2]Department of Biology, University of Genova, Genova, Italy
[3]Department of Oncology Biology and Genetics, University of Genova, Genova, Italy
[4]Department of Experimental Medicine and Pathology, II Faculty of Medicine, University of Roma "La Sapienza", Roma, Italy

Abstract   Ataxia telangiectasia (AT) is a rare genetic disorder caused by mutations of *ATM* gene. ATM kinase is a "master controller" of DNA-damage response and signal transducer of external stimuli. The complex role of ATM may explain the pleiotropic phenotype characteristic of AT syndrome, only partially. In our hypothesis, the multi-faceted phenotype of AT patients might depend on specific chromatin reorganization, which then reflects on the cellular transcription. We analyzed three lymphoblastoid cell-lines isolated from AT patients and one healthy control. The three-dimensional reconstruction disclosed marked changes of nuclear morphology and architecture in AT cells. When chromatin condensation was analyzed by differential scanning calorimetry, a remodeling was observed at the level of fiber folding and nucleosome conformation. Despite the structural differences, chromatin did not exhibit modifications of the average acetylation status in comparison to the control. Moreover, AT cells presented significant alterations in the transcription of genes involved in cell-cycle regulation and stress response. In AT3RM cells, the average chromatin decondensation went with the upregulation of c-fos, c-jun, and c-myc and downregulation of metallothioneins, p21 and p53. AT9RM and AT44RM cells were instead characterized by an increased chromatin condensation and presented a different transcription unbalance. Whereas in AT44RM all the considered genes were downregulated, in AT3RM the three oncogenes and metallothioneins were upregulated, but p53 and p21 were downregulated. J. Cell. Biochem. 99: 1148–1164, 2006.   © 2006 Wiley-Liss, Inc.

Key words: ataxia telangiectasia; nuclear architecture; chromatin structure; gene transcription

Cell nucleus is a dynamic compartment where chromatin fibers exhibit high flexibility [Bubulya and Spector, 2004; Ehrenhofer-Murray, 2004]. Changes of chromatin folding can modify the accessibility of the DNA sequences to transcription factors. Rearrangements in chromatin structure, in fact, are known to collaborate with classical regulatory elements to modulate gene expression [Workman and Kingston, 1998; Stein et al., 1999]. At the level of low-order chromatin structure, nucleosomes can be switched on from a closed to an open conformation by remodeling complexes [Polach and Widom, 1995; Cosma et al., 1999], histone modifications [Marmorstein, 2001; Lachner et al., 2003], DNA supercoiling [Vergani et al., 1994]. Also the large-scale chromatin organization seems to participate in the control of gene expression [Belmont et al., 1984; Belmont et al., 1999; Cremer and Cremer, 2001; Cremer et al., 2003]. Many evidences demonstrated as nuclear architecture changed during cell differentiation [Marshall, 2003] and in response to cell shape alterations [Vergani et al., 2004] or hormone

exposure [Nye et al., 2002]. However, it remains unclear how changes in the three-dimensional chromatin organization might affect the gene expression.

We investigated the three-dimensional chromatin organization and the pattern of gene expression in lymphoblastoid cell-lines isolated from patients affected by ataxia telangiectasia (AT), a progressive neurodegenerative disorder caused by mutations of the *ATM* gene. The ATM serine/threonine kinase belongs to the phosphoinositide 3-kinase like kinase (PIKK) family. ATM is involved in the response to DNA damages, cell-cycle control, and in the maintenance of the genomic integrity [Savitsky et al., 1995a,b; Abraham, 2001; Shiloh and Kastan, 2001]. ATM acts as an early sensor and activator of the cellular responses to double-strand DNA breaks (DSBs) [Shiloh, 2003]. Following DNA damages, ATM autophosphorylates on serine 1981 and, as consequence, the inactive dimeric/multimeric form dissociates into the active monomers [Goodarzi and Lees-Miller, 2004]. Recent evidences suggested that ATM is also activated by physiological events, such as the chromatin remodeling occurring during transcription [Bakkenist and Kastan, 2003]. Activation of ATM results in phosphorylation of many substrates, including p53, and triggers cell-cycle arrest at G1/S, intra-S, or G2/M phase [Kurz and Lees-Miller, 2004] or, alternatively, induces apoptosis. However,

ATM controls also pathways not directly associated with DNA damage [Xu et al., 1996; Lim et al., 1998; Guo et al., 1999; Smilenov et al., 1999].

The majority of *ATM* mutations give rise to a truncated unstable protein or no product at all. Mutations include large or small in-frame deletions, insertions, and substitutions [Gilad et al., 1996; Concannon and Gatti, 1997; Sandoval et al., 1999; Abraham, 2001]. The clinical phenotype of AT patients is characterized by cerebellar ataxia, ocular telangiectasia, oculomotor apraxia, immunodeficiency, and cancer susceptibility [Shiloh, 2003]. AT cells show also severe chromosomal aberrations [van Gent et al., 2001], genomic instability, radio-resistant DNA synthesis [Shiloh, 2003], hypersensitivity to ionizing radiations, and oxygen radicals [Rich et al., 2000].

The role of ATM as a hierarchical kinase (Fig. 1) explains how it can impact many pathways at once. However, the relationship between phenotype severity and kind of *ATM* mutation is still unclear. Previous studies carried out by Vergani et al. [1999]; Djuzenova and Flentje [2001]; Grattarola et al. [2003] reported strong evidences of an altered chromatin condensation in AT cells. Also in meiosis the nuclear architecture is affected by *ATM* mutations, since *ATM* mutants show an immature heterochromatin distribution [Scherthan et al., 2000]. Moreover, Hittelman and Pandita
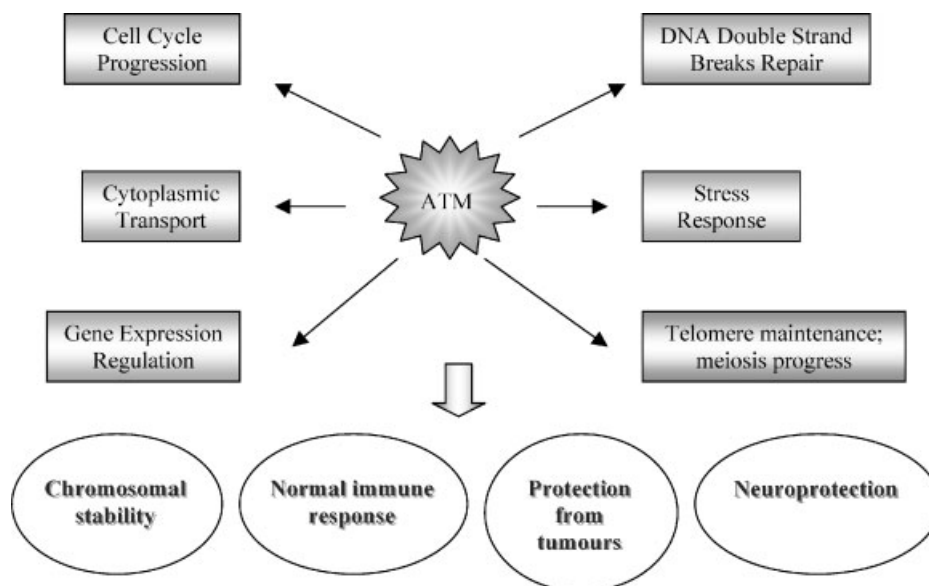

Fig. 1. Role of ATM in the physiological signaling network.

[1994] suggested that the chromatin alterations characteristic of AT cells might cause a more probable conversion of DSBs into chromosome damage.

These data strengthened our opinion that rearrangements of chromatin structure may represent a central event of AT disorder and induce a wide-range of down-stream effects, in particular at the level of gene transcription. We hypothesized that the chromatin remodeling occurring in AT cell-lines is strictly related to the kind of *ATM* mutation.

In this study we analyzed three lymphoblastoid cell-lines isolated from homozygous AT patients and one healthy control. The AT cell-lines were selected on the basis of the *ATM* mutation: a large deletion in AT44RM [Gilad et al., 1996], a single substitution $C \rightarrow T$ in AT9RM, a mutation not yet identified in AT3RM cells, which nevertheless exhibit a classical AT phenotype lacking of ATM protein. The healthy control was a relative of the AT44RM patient with wild-type ATM genotype. For each cell-line the three-dimensional nuclear architecture was analyzed, by determining the localization of the highly condensed domains, the texture, and granularity of the chromatin. We determined also the average chromatin condensation, the level of histone acetylation, and the fraction of the actively transcribed nucleosomes. As last point we analyzed the gene transcription pattern. In this preliminary approach we focused on a limited number of genes: two transcription factors laying under the control of ATM, the tumor-suppressor genes p53 [Kastan et al., 1992] and p21 [Boulaire et al., 2000], three oncogenes, c-myc, c-jun, and c-fos, and two stress proteins, the metallothionein 1A and 2A [Beattie et al., 2005].

MATERIALS AND METHODS

Cell Cultures

Four lymphoblastoid cell-lines immortalized by Epstein Barr virus were supplied by the "Cell Repository of the Italian Registry for Ataxia Telangiectasia" [Chessa et al., 1994]. Three lines derived from AT patients (AT44RM, AT3RM, AT9RM) and one from an intrafamilial wild-type control (243RM). Cells were grown in RPMI 1640 medium supplemented with foetal calf serum 10% and gentamycin 0.1 mg/ml (Sigma, Milano, Italy). The cultures were maintained at 37°C with 5%

CO_2 atmosphere. Before the experiments cells were synchronized at the G1/S phase of the cell-cycle by incubation with hydroxiurea 2 mM for 15 h.

Fluorescence Microscopy

Nuclear architecture and chromatin organization were visualized by cell staining with 4′, 6-diamidino-2-phenylindole (DAPI), a fluorescent dye selective for dsDNA. After fixation in 2% glutharaldehyde, cells were incubated with 15 μM DAPI in a buffer preserving the 3D structure of the nucleus (80 mM KCl, 20 mM NaCl, 2 mM Na_2EDTA, 0.5 mM EGTA, 15 mM pipes, 1 mM PMSF, 0.5 mM spermidine, 0.2 mM spermine, β-mercaptoethanol 0.12% [Belmont and Bruce, 1994]. An Axioplan light microscope (Zeiss, Oberoken, Germany) equipped with Zeiss Plan-Neofluar objective lens was used to observe the cells. Digitalized images were obtained from an air-cooled (−50°C) scientific grade CCD camera (ORCA II Hamamatsu Photonics, Japan), with a dynamic range of 14 bits (grey levels 0–16,383). Calibration for defects in bi-dimensional illumination and CCD array homogeneity was performed [Hiraoka et al., 1987]. Optical sectioning of the single nuclei was carried out by acquiring a stack of 128 nuclear images at different focal positions along the z-axis (0.1 μm intervals). Shading correction and dark image subtraction were applied to each image [Mascetti et al., 1996]. The out-of-focus contributions were removed by applying the nearest-neighbor algorithm [Agard, 1984] and a constrained deconvolution was applied to sharpen the image [Agard et al., 1989; Mascetti et al., 2001]. The 3D reconstruction was performed by AMIRA 2.2 software (http://www.amiravis.com).

Differential Scanning Calorimetry

Native nuclei were prepared by extraction in hypotonic buffer as previously described [Nicolini et al., 1988a]. DSC experiments were performed on a Perkin Elmer DSC instrument (Perkin Elmer, Monza, Italy) with 100 μl stainless-steel capsules in the temperature range 310–410 K using standard parameters [Nicolini et al., 1988b]. At least three different measurements for each sample were made in order to check accuracy and statistical significance of the experiment. The relative melting enthalpy of each thermal transition was calculated by decomposing the heat capacity profile

into its Gaussian components through a least square fitting algorithm [Bartels, 1979].

Flow Cytometry

Lymphoblastoid cells were collected, washed, and fixed with a solution of glutaraldehyde 2%, $MgCl_2$ 2 mM, and EGTA 2 mM in PBS $1\times$ pH 7.35 for 45 min. Then cells were briefly permeated with Triton 1%, washed and incubated O/N with the primary antibody against the acetylated H4 (Upstate Biotechnology, Milan, Italy). After washing, cells were incubated with the IgG-FITC-conjugated secondary antibody (Santa Cruz Biotechnology, Santa Cruz, CA) in the dark. Green fluorescence was measured by FACS and analyzed using Cell Quest Software (Becton Dickinson).

Mononucleosome Preparation and Separation

Mononucleosomes were extracted according to a standard procedure [Allegra et al., 1987]. Nuclei were digested with 8 U/ml micrococcal nuclease for 7 min at 37°C. The supernatant containing the mononucleosomes was applied on an organomercurial-agarose column (Bio-Rad, Milan, Italy), where the Hg atoms selectively retained the sulfhydryl groups through mercaptide bonds. Because transcriptionally inactive mononucleosomes have a folded conformation with the SH group of histone H3 partially or completely shielded, they are not retained on the resin. On the contrary in active nucleosomes the SH group is accessible [Walker et al., 1990; Gavazzo et al., 1997; Vergani et al., 2004] and they are retained selectively on the resin and displaced with the addition of 10 mM dithio-

threitol. The elution profile was monitored recording absorbance at 260 nm.

RNA Extraction and RT-PCR

Total RNA was extracted by the acid phenol–chloroform procedure according to Chomczynski and Sacchi [1987]. Concentration and purity of the RNA was determined by absorption spectrophotometry. Quality of the RNA was checked by electrophoretic run on 1.5% agarose. RNA was retrotranscribed using 201 pmol oligo dT18 (TIB MOLBIOL, Genoa, Italy), 30 units AMV, 40 units RNAsin, and 1mM dNTPs (Promega, Madison) in a total volume of 20 µl at 42°C for 45 min. The sequence of interest was amplified by PCR reaction using 0.25 µM sense and anti-sense primers, 200 µM each dNTPs, 1.5 units of TAQ polymerase, $1\times$ TaQ Buffer, 2 mM $MgCl_2$ (TIB MOLBIOL). The primers pairs were designed using a free package [Rozen and Skaletsky, 2000]. Table I resumes for each primer pair the sequence, the annealing temperature, and the extension length of the PCR reaction. The general PCR scheme was the following: denaturation at 94°C for 5 min, 25–35 cycles of amplification (94°C for 1 min, annealing and extension at 72°C), and final extension at 72°C for 10 min. For each gene we started from 20 and we arrived to 35 cycles, to verify to be in the exponential phase of amplification. After running on 1.5% agarose gel, the amplified sequence was evaluated by measuring the optical density of the electrophoretic band by means of Image J. 1.24 free software (National Institute of Health, Bethesda; http://rsb.info.nih.gov/ij/).

TABLE I. Sequences of the Primer Pairs Used in the RT-PCR Experiment

Genes	Primer pairs	Transcript length (bp)	Annealing (°C and s)	Extension (s)
p53	CCT GCC CTC AAC AAG ATG TTT TG TCA AAG CTG TTC CGT CCC AG	431	60°C (45 s)	1 min 30 s
p21	CTG CCC AAG CTC TAC CTC CC CAG GTC CAC ATG GTC TTC CT	121	65°C (60 s)	45 s
c-myc	ACC ACC AGC AGC GAC TCT G CTA CCT TGG GGG CCT TTT C	442	66°C (60 s)	1 min 20 s
c-fos	GAC TAC GAG GCG TCA TCC TCC C CTC TGG TCT GCG ATG GGG CCA C	250	67°C (70 s)	1 min
c-jun	CCC AAG AAC GTG ACA GAT GA CAC TGT CTG AGG CTC CTC CT	399	50°C (45 s)	1 min
MT1A	ACT GGT GGC TCC TGC ACC TGC ACT ACA GCA GCT GCA CTT CTC TGA T	175	59°C (60 s)	1 min
MT2A	GCC GGT GAC TCC TGC ACC TGC G GCA GCA GCT GCA CTT GTC CGA C	175	61°C (60 s)	1 min
β-actin	TGA CGG GGT CAC CCA CAC TGT GCC CAT CTA CTA GAA GCA TTT GCG GTG GAC GAT GGA GGG	661	60°C (45 s)	1 min 30 s

The primers for p21, MT1A, and MT2A were from the literature [Schonherr et al., 2001; Bianchi et al., 2002] while the primers for p53 and β-actin have been taken from Stratagene. The primers for the other genes were designed on the basis of the complete cDNA sequences using the Primer3 free software [Rozen and Skaletsky, 2000].

Immunoblot Analysis

Whole cell extracts were prepared as previously described [Marchi et al., 2005] by lysis in boiling Laemmli SDS-buffer. Protein concentration was determined using Bradford protein assay reagent and bovine serum albumin as standard [Bradford, 1976]. Samples (20–30 μg for lane) were electrophoresed on 12% SDS–PAGE under reducing conditions [Laemmli, 1970] and transferred to nitrocellulose membranes (Amersham, Uppsala, Sweden). For detection of metallothioneins, samples were reduced with 1% β-mercaptoethanol before electroforesis. After run the gel was incubated for 20 min at room temperature in methanol/CAPS buffer (10% methanol in 10 mM CAPS, pH 11) supplemented with 2 mM $CaCl_2$ and electroblotted in the same buffer [Mizzen et al., 1996]. Membranes were then probed with a rabbit polyclonal anti-MT antibody (Santa Cruz) diluted as primary antibody, and horseradish-peroxidase-conjugated goat anti-rabbit IgG as secondary antibody. Blots were stripped by incubation in stripping buffer (100 mM β-mercaptoethanol, 2% SDS, 62.5 mM Tris-HCl, pH 6.7) for 30 min at 50°C. Thereafter, blots were incubated with blocking buffer and reprobed with anti-actin antibodies (Sigma). Binding of antibodies was visualized by enhanced chemiluminescence (ECL) detection system (Roche, Milan, Italy) on hyperfilm ECL (Amersham), and bands were quantified using ImageJ 1.31v, image analysis free software (http://rsb.info.nih.gov/ij/). Each band was therefore converted into a densitometry trace allowing calculations of peak area and intensity. The results were expressed as a ratio to the densitometry area for the actin band from the same sample.

Statistics

Data from different experiments are expressed as means ± SEM and they have been compared by Student's t-test. Differences are considered significant at $P < 0.05$.

RESULTS

Nuclear Architecture and Morphometry

A stack of 128 nuclear sections of a single cell was recorded to reconstruct the 3D structure of the nucleus. At least five different nuclei were acquired for each line and the most representative were reported in Figure 2. From the stack, the AT3RM nucleus appears clearly enlarged and the fluorescence distribution is more diffuse than in the healthy cells, where the highly intensity chromatin domains are localized preferentially at the periphery (Fig. 2A,B). In AT9RM and AT44RM (Fig. 2C,D), instead, the nuclear size and morphology do not show significant alterations in comparison with the control. The major difference observed in AT9RM is the distribution of the highly condensed domains across the entire nucleus and not confined at the nuclear periphery, as in the control cells.

From the 3D reconstruction of the same nuclei we can appreciate some further details. In particular, the healthy cell-line shows a marked compartmentalization of the chromatin domains (Fig. 3A): the highly condensed fibers, which exhibit a higher fluorescent intensity [Mascetti et al., 2001], are arranged one close to the other to form a continuous structure localized preferentially at the nuclear periphery. In AT3RM cells (Fig. 3B) the highly condensed domains are reduced in number and size and form a loose network and chromatin reduces its granularity assuming a more homogeneous texture. In AT9RM nucleus (Fig. 3C) the highly condensed domains are preserved, even if rearranged with a movement from the periphery towards the center. The highly condensed regions are distributed over the entire nucleus and not confined at the periphery, as in 243RM cells. Also in AT44RM (Fig. 3D) the nuclear architecture is rearranged, and the chromatin domains close to the envelope assume a more trabeculated organization. In fact, the macrofibrils are more evident in AT44RM than in the control and they diffuse towards the center, where form a large condensed domain.

The data recorded at the single cell level have been integrated by recording the morphometric parameters of more than 30 nuclei per line at a lower magnification (Table II). Compared to the control, AT3RM cells show an increase of nuclear perimeter (from 39 to 51 μm) and area (from 118 to 194 $μm^2$). Since the nuclear images are bi-dimensional projections of a three-dimensional object, this increase of the 2D area corresponds to an increase of the 3D volume, on condition that the thickness of the object does not change. Since previous reports demonstrated an inverse relationship existing
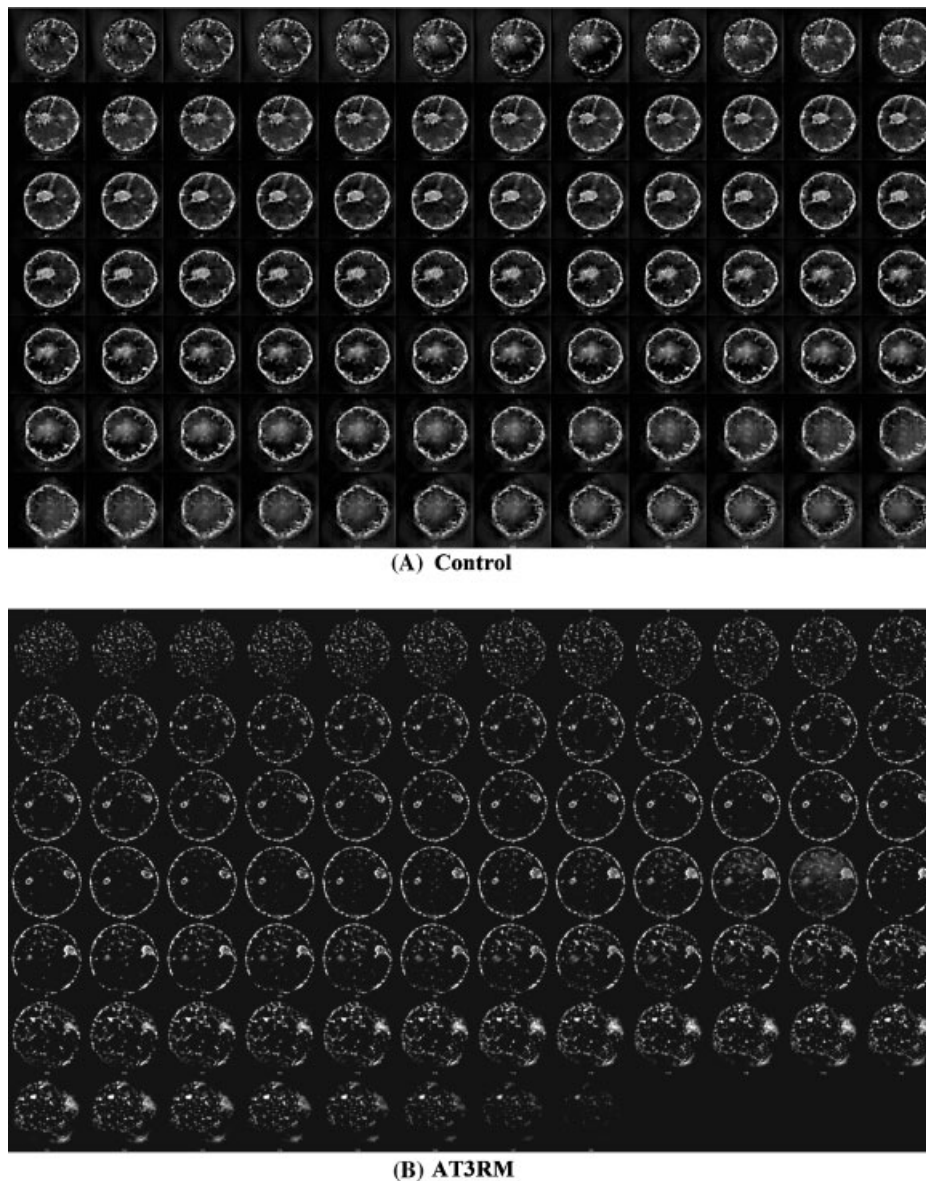
(A) Control

(B) AT3RM

Fig. 2. Representative stack from the four lymphoblastoid nuclei: (**A**) Control, (**B**) AT3RM, (**C**) AT9RM, (**D**) AT44RM. The stacks of 128 nuclear images were acquired at different focal positions along the z-axis after selective staining of the nuclear DNA with DAPI.
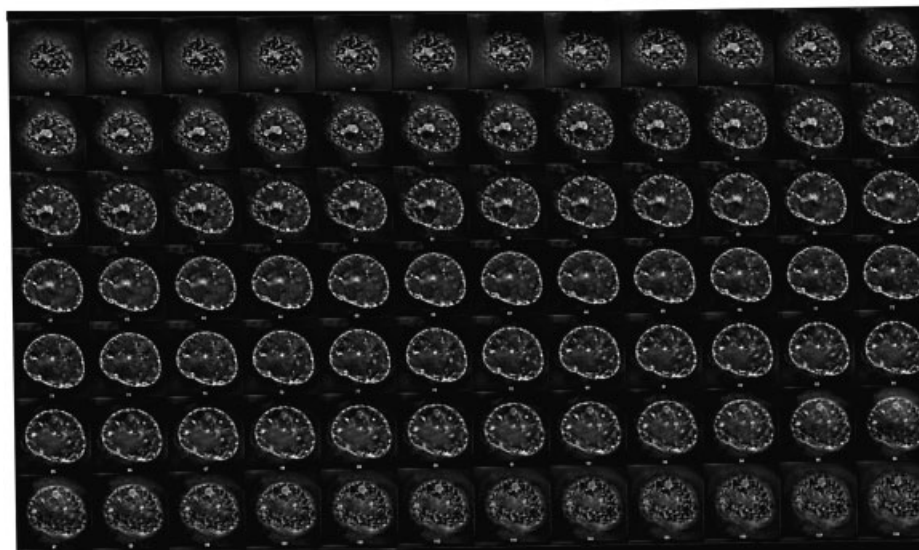
between chromatin condensation and nuclear volume [Belmont et al., 1984; Haussinger, 1996; Mascetti et al., 2001], an enlarged nuclear volume should be associated with an average unfolding of chromatin fibers and, in fact, the 3D reconstruction showed a reduced granularity of the chromatin in AT3RM cells. On the contrary, in AT9RM cells the perimeter and area decrease till to 33 μm and 81 μm^2, respectively. Finally, AT44RM cells exhibit values of nuclear perimeter and area rather similar to those of control, pointing to only

marginal modifications occurring in this AT line at the level of chromatin architecture and folding.

From these results we can infer as a reorganization of nuclear architecture occurs in all the AT cell-lines under analysis with relapses on the nuclear morphometry. In conclusion, while in AT44RM cells the nuclear architecture and size are rather similar to the control, in AT3RM and AT9RM these features result significantly altered, even if in the opposite directions.
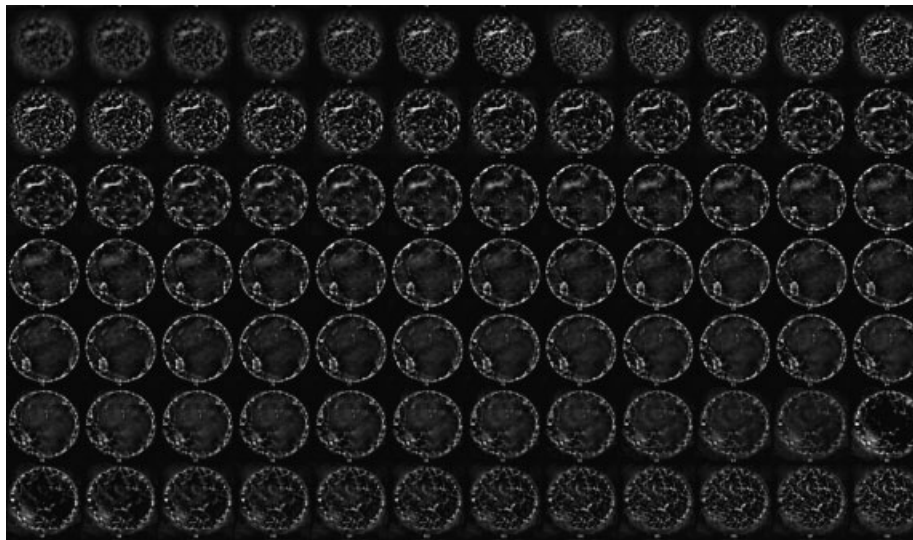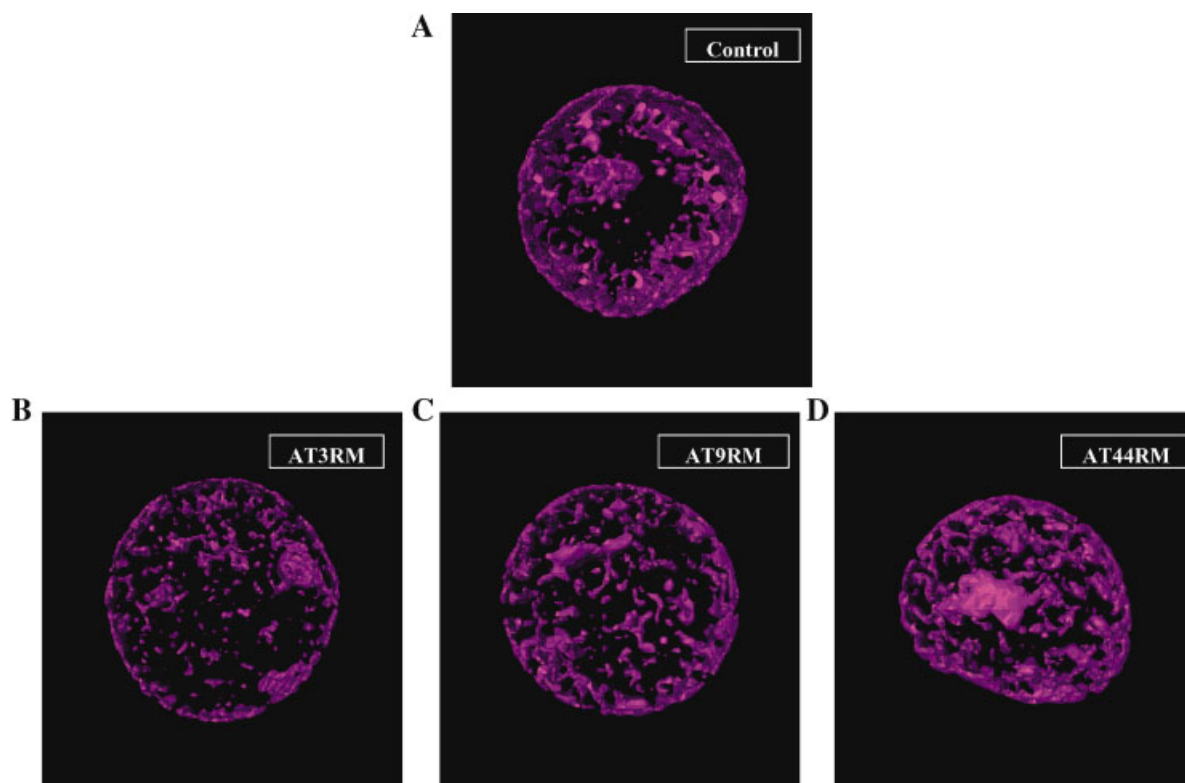
(C) AT9RM

(D) AT44RM

Fig. 2. (*Continued*)

Chromatin Remodeling

The rearrangements above described in nuclear architecture led us to hypothesize changes of chromatin condensation associated with the different *ATM* mutations. Therefore the high- and low-order chromatin structure was analyzed in the four lymphoblastoid lines. Differential scanning calorimetry is commonly employed to determine in situ the structural changes of chromatin associated with physiological or pathological events, such cell-cycle progression [Nicolini et al., 1988a; Nigg et al.,

1996], neoplastic transformation [Zink et al., 2004], environment conditions [Vergani et al., 1998; Vergani et al., 2004]. As widely described [Touchette and Cole, 1985; Nicolini et al., 1988; Balbi et al., 1989] the thermal denaturation profile of native mammalian nuclei usually exhibits four main transitions: Transition 0 centered at about 330 K corresponding to melting of membranes and debris, Transition I at 335 K corresponding to denaturation of nuclear proteins, Transition II at 357 K to DNA of nucleosome organized in 10 nm filament, and Transition III at about 370 K to DNA

Fig. 3. Three-dimensional reconstruction of the four lymphoblastoid nuclei: (**A**) Control, (**B**) AT3RM, (**C**) AT9RM, (**D**) AT44RM. The three-dimensional organization of chromatin domains was visualized both for the control (243RM) and the AT cells. For each cell-line a nucleus representative of the entire population was reported. The images were acquired at high resolution using a 100× objective and the 3D reconstruction was obtained by elaborating the stack of 128 images acquired at different focal positions along the z-axis. [Color figure can be viewed in the online issue, which is available at www.interscience.wiley.com.]

of nucleosome organized in higher-order structures as fibers of 30 nm or more. This general assignment has been verified in the human lymphoblasts under analysis [Grattarola et al., 2003], confirming that Transition III represents the melting of highly condensed chromatin, while Transition II is associated to the melting

of uncondensed chromatin domains. The Gaussian decomposition of Transition II revealed two sub-components centered at 355 and 359 K, assigned to the melting of linker and core DNA, respectively, while Transition III yielded two components centered at 367 and 372 K representing the melting of chromatin fibers with different degrees of condensation [Allera et al., 1997; Vergani et al., 1998, 1999].

First of all we assessed the internal variability of the samples by acquiring the thermograms of three different cell-lines all deriving from healthy relatives of the AT patients (data not shown). The analysis supplied a good reproducibility of the thermal profiles among the different samples, with a very low internal variability.

In Table III, we listed the values of the relative melting enthalpy calculated for all transitions and sub-transitions appearing in the thermograms. In comparison with the healthy control, all AT cell-lines exhibit significant alterations in the heat capacity profile

TABLE II. Morphometric and Intensitometric Parameters Recorded for the Three AT cell-lines (AT3RM, AT9RM, and AT44RM) and the Healthy Control (243RM) by Fluorescence Microscopy

Cell-lines	Nuclear area (μm^2)	Nuclear perimeter (μm)	Form factor
243RM	118 ± 17	39 ± 6	0.95 ± 0.26
AT3RM	194 ± 27	51 ± 8	0.94 ± 0.26
AT9RM	82 ± 7	33 ± 5	0.96 ± 0.23
AT44RM	114 ± 13	39 ± 6	0.93 ± 0.25

Form factor corresponds to area divided by the perimeter squared ($4\pi A/P^2$) [Belmont et al., 1980]. More than 30 nuclear images were acquired for each sample and the standard deviation was reported.

TABLE III. The Relative Melting Enthalpies of the Transitions II and III Were Estimated on the Thermograms Recorded for the Healthy Control (243RM) and the Three AT Cells (AT3RM, AT9RM, and AT44RM)

Cell-lines	II_{Tot} 356 ± 2 K	II_a 354 ± 2 K	II_b 359 ± 1 K	Ratio II_a/II_b	III_{Tot} 371 ± 1 K	III_a 369 ± 1 K	III_b 375 ± 2 K	Ratio III_a/III_b
243RM	0.42 ± 0.06	0.10 ± 0.01	0.32 ± 0.05	0.32	0.54 ± 0.08	0.45 ± 0.07	0.10 ± 0.01	4.50
AT3RM	0.44 ± 0.05	0.10 ± 0.02	0.34 ± 0.04	0.29	0.49 ± 0.07	0.42 ± 0.06	0.05 ± 0.01	8.40
AT9RM	0.33 ± 0.05	0.12 ± 0.03	0.21 ± 0.03	0.59	0.65 ± 0.09	0.41 ± 0.05	0.24 ± 0.04	1.70
AT44RM	0.21 ± 0.02	0.11 ± 0.01	0.11 ± 0.02	1	0.73 ± 0.11	0.51 ± 0.08	0.22 ± 0.05	2.31

The relative melting enthalpies of each sub-transition were also reported together with their ratio. The experiments have been repeated at least three times for each cell-line and the standard deviations were <15%.

(Fig. 4). AT3RM nuclei show an enhancement of Transition II (from 0.32 to 0.44 AU) and a reduction of Transition III (from 0.54 to 0.49 AU), which point to an average unfolding of the highly condensed chromatin fibers. This result perfectly matches with the enlarged nuclear size observed in the 3D-reconstructed nucleus (Fig. 3) and quantitatively measured on the 40× images (Table II). Also the sub-components result modified with respect to the control: a marked decrement of the II_a/II_b ratio (from 0.31 to 0.28) is balanced by an increment of the III_a/III_b ratio (from 4.65 to 8.98). These data indicate as the average decondensation occurring at the level of the chromatin high-order structure is associated to an opposite change at the level of nucleosomes, which assume a more folded conformation. Also, AT9RM supply a thermogram modified with respect to control, even if opposite with respect to AT3RM cells. The thermal denaturation profile, in fact, exhibits

an evident decrease of Transition II (relative enthalpy from 0.42 to 0.33) that is balanced by the increase of Transition III (from 0.54 to 0.65), suggesting an average chromatin condensation occurring in this cell-lines. The sub-components are modified too, with an increase of the II_a/II_b ratio (from 0.31 to 0.59) and a decrease of the III_a/III_b one (from 4.6 to 1.73). Also in this case, the structural changes appear different when the low- and the high-order chromatin structures are observed. While nucleosomes show a partial unfolding, on the contrary the 30 nm chromatin fibers fold into more condensed structures. The thermogram of AT44RM exhibits changes rather similar to those observed for AT9RM: Transition II in fact considerably decreases (enthalpy from 0.42 to 0.24), and Transition III increases (enthalpy from 0.54 to 0.73). Sub-transitions are also modified, with the II_a/II_b ratio increasing from 0.31 to 1 and the III_a/III_b ratio decreasing from 4.65 to 2.27. In
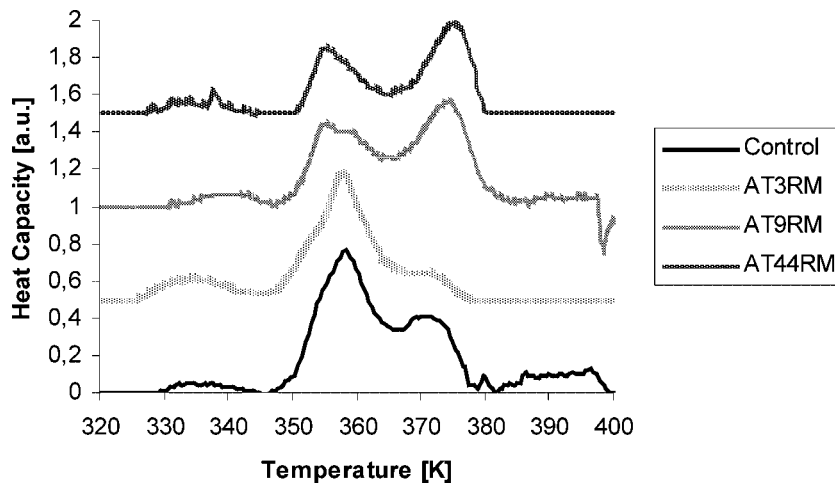
Fig. 4. Thermograms of the four cell-lines. The thermal denaturation profiles of native nuclei isolated from the four cell-lines under analysis were compared to deduce structural information about in situ chromatin. The thermograms report heat capacity (AU) versus temperature (K) for control 243RM, AT3RM AT9RM, and AT44RM cells.

spite of the similar changes at the level of chromatin condensation, AT44RM does not show the alterations of nuclear volume observed for the AT9RM cells (Fig. 3 and Table II).

In conclusion, a marked chromatin remodeling is evident in all three lymphoblastoid lines affected by homozygous mutations of the *ATM* gene. Nevertheless, while the AT44RM and the AT9RM exhibit an average chromatin condensation, the AT3RM cells present instead an average chromatin decondensation.

Chromatin Acetylation

The changes of chromatin structure and nuclear architecture are usually associated with post-translational modifications of the octamer histones. Therefore, we evaluated the average acetylation status of the chromatin in the four cell-lines by immunofluorescence labeling of the acetylated form of the histone H4. The three fluorescence histograms obtained by cytofluorimetry of the AT lines appear to be very similar to the healthy control (Fig. 5), suggesting that no quantifiable modifications occur in the chromatin acetylation as a consequence of the *ATM* mutations. These results were confirmed when the acetylated form of histone H4 was quantified by immunoblot (data not shown). Our data are consistent with the recent observations of other authors [Gupta et al., 2005]. A last consideration has to be made:

although the cytofluorimetric analysis does not show changes of the chromatin acetylation status on average, the existence of different levels of acetylation in specific regulatory sequences cannot be ruled out.

Nucleosome Conformation

The calorimetric data revealed as the chromatin remodeling associated with the *ATM* mutations affected also the nucleosome conformation. By affinity chromatography we separated active from inactive nucleosome particles inside the entire population of transcriptable nucleosomes. Whereas transcriptionally active nucleosomes were retained on the matrix (II peak), inactive ones were eluted directly (I peak) [Allfrey and Chen, 1991; Gavazzo et al., 1997; Vergani et al., 2004]. In Table IV we listed the average fractions of active and inactive nucleosomes on the overall nucleosome population. With respect to the control, in all AT lines we observe a general increase of transcriptionally inactive nucleosomes. In all the samples (Fig. 6) the I peak, in fact, is higher than the II peak, even if the differences are not significant. A reduced fraction of the actively transcribed nucleosomes in AT3RM is in accordance with the more compact nucleosome conformation recorded by differential scanning calorimetry. On the contrary, in AT9RM and AT44RM this datum does not fit with the calorimetric results,
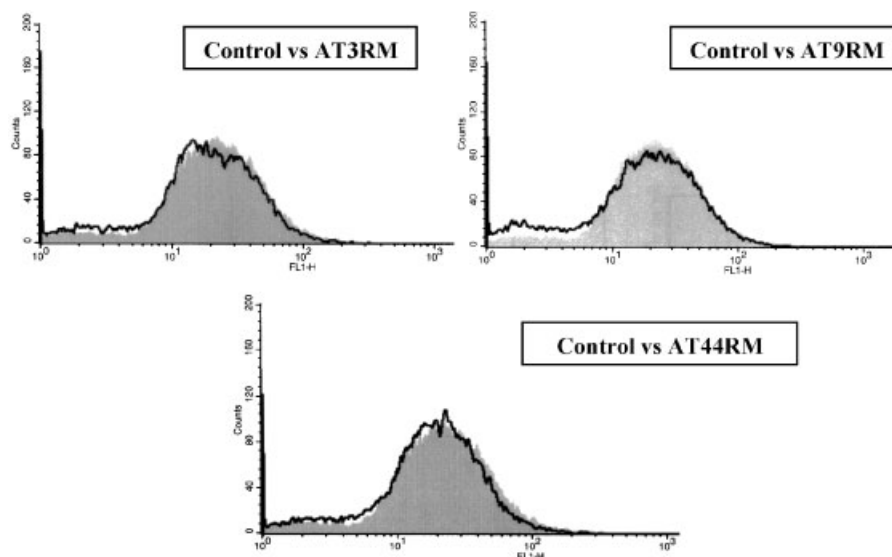
Fig. 5. Immunofluorescence labeling of the acetylated histone H4. The fluorescence histogram acquired for the healthy control (243RM ▣) was compared with those of AT cells (━━): AT3RM, AT9RM, and AT44RM. The x-axis (FL1-H) represents the green fluorescence associated to the H4 acetylation; the y-axis (counts) corresponds to the events number.

TABLE IV. Fractions of Transcriptionally Inactive Nucleosomes Eluting at Physiological Ionic Strength (I Peak) and Fractions of Active Ones Eluting After Addition of DTT (II Peak) are Summarized

Cell-lines	I peak (inactive nucleosomes)	II peak (active nucleosomes)
243RM	0.74 ± 0.09	0.23 ± 0.09
AT3RM	0.79 ± 0.02	0.20 ± 0.03
AT9RM	0.81 ± 0.03	0.17 ± 0.02
AT44RM	0.80 ± 0.03	0.19 ± 0.03

The fractions have been determined for each cell-line by an affinity chromatography.

which indicated an average unfolding of the nucleosome particles. This apparent discrepancy can depend on the nucleosome population analyzed. While the calorimetric data regarded the entire nucleosome population of the nuclei, the chromatographic separation was carried out on a nucleosome sub-population, namely the potentially transcriptable nucleosomes, which were selectively extracted from the nuclei by discarding the bulk of the silent nucleosomes.

Gene Expression

From the above results we can conclude that both single substitutions and large or short deletions in *ATM* gene affect the nuclear architecture and chromatin structure of the cells. A further question was still open: do the structural changes observed in chromatin and nucleosome conformation reflect on the gene expression profile of the cells? On the light of the

genetic instability and tumor predisposition characteristic of AT syndrome, our initial approach focused on genes involved in the maintenance of cell homeostasis.

In Figure 7 we reported for every gene the relative expression calculated with respect to housekeeping gene. The tumor-suppressor gene p53 is downregulated in AT3RM and AT44RM, while it is not modulated in AT9RM. Similar changes are observed for p21, a transcription factor directly regulated by p53 [Vogelstein and Kinzler, 2004].

The oncogene c-myc is significantly upregulated in AT3RM and AT9RM and downregulated in AT44RM. Because of the role of c-myc in the cell-cycle progression, these data perfectly match with the growth curves recorded for the AT lines (data not shown), AT44RM supplied, in fact, a slower growth with respect to the other three lines. The upregulation of c-myc transcription in AT3RM and AT9RM suggests higher risk of neoplastic transformation in these cell-lines. It is comforting that a similar transcriptional modulation was observed for the oncogenes c-fos and c-jun, members of the AP1 complex [Shaulian and Karin, 2002]. They are upregulated in AT9RM, and especially in AT3RM cells, whereas they are downregulated in AT44RM.

In conclusion, AT9RM and AT3RM cell-lines seem to posses an increased AP1 activity, in accordance to previous in vivo results [Weizman et al., 2003]. We can hypothesize that this
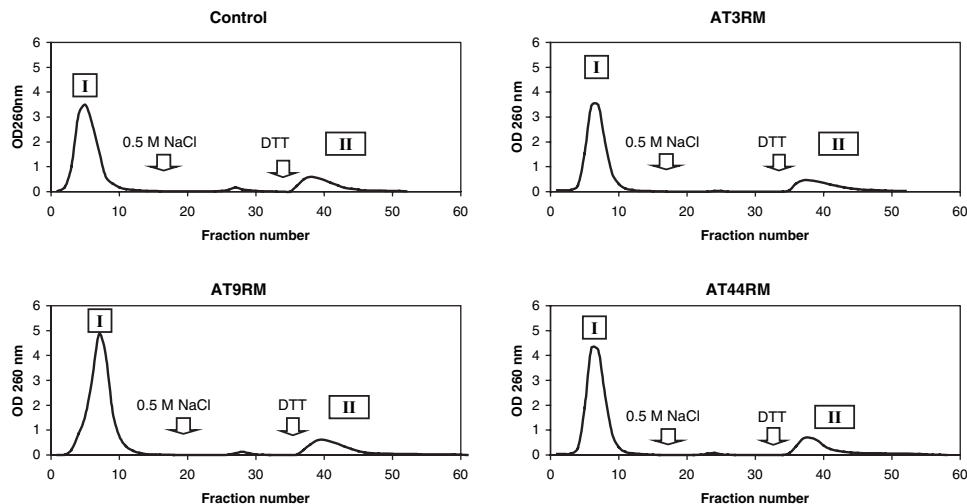
Fig. 6. Fractionation of nucleosomes by Hg-agarose affinity chromatography. Nucleosomes released by limited micrococcal nuclease digestion of isolated nuclei were recovered from control cells and AT3RM, AT9RM, AT44RM cells. An organomercurial-agarose affinity chromatography allowed us to estimate the fraction of transcriptionally active mononucleosomes from inactive ones.
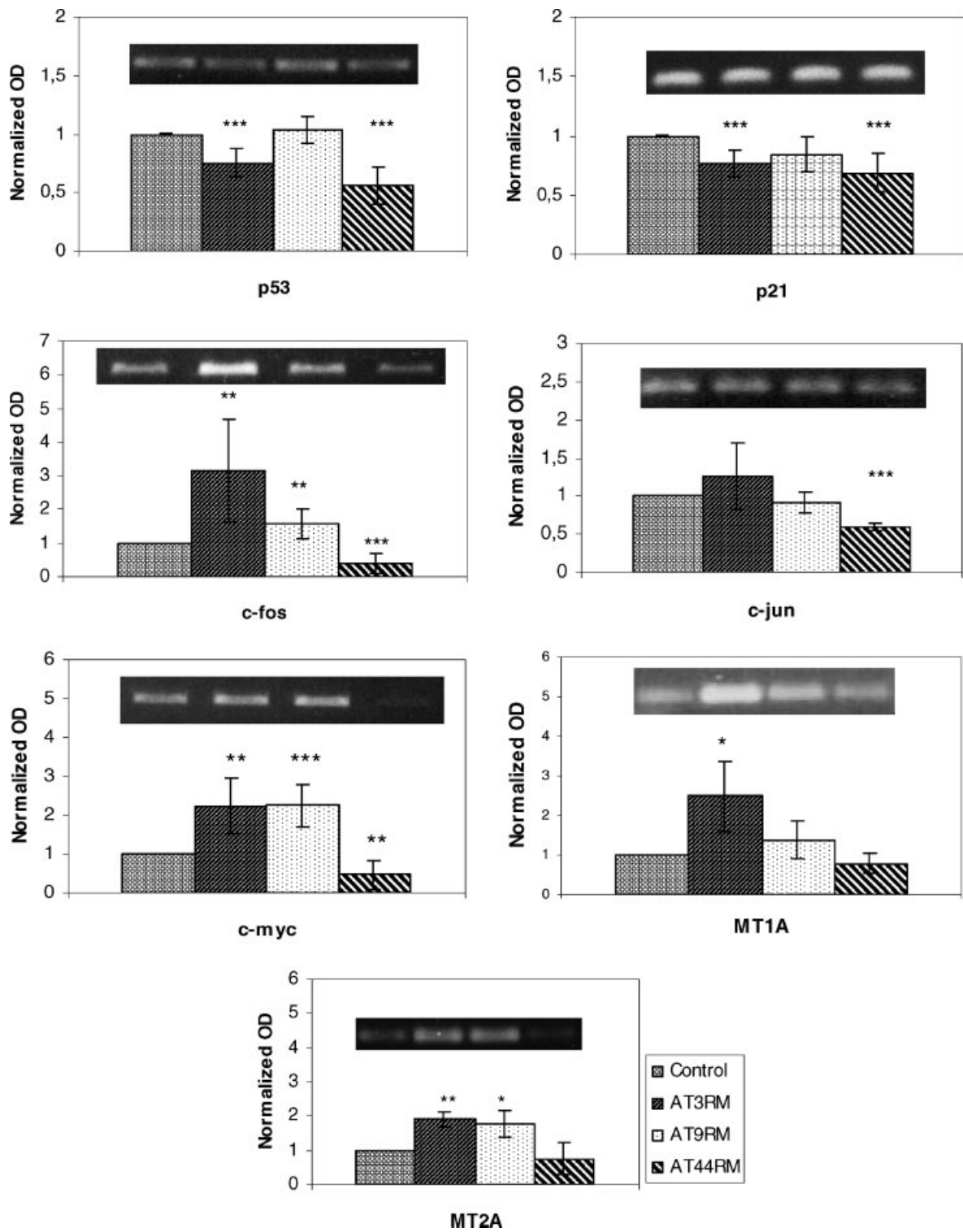
Fig. 7. Gene expression pattern. The transcription of seven genes (p53, p21, c-myc, c-jun, c-fos, MT1A, MT2A) was analyzed for the healthy control, 243RM cells, and the three AT cell-lines (AT3RM, AT9RM, and AT44RM) using semi-quantitative RT-PCR. Each value, with the relative standard deviation, was the averages of at least three different independent measurements. Asterisks indicate values significantly different from those of control at *$P < 0.05$, **$P < 0.01$, ***$P < 0.001$.
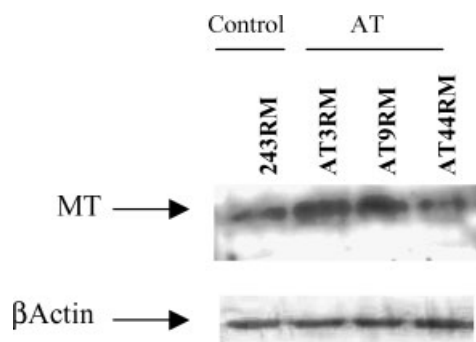
Fig. 8. Basal level of metallothionein proteins in AT and control cell-lines. Immunoblotting analysis was performed using antibodies against MTs as described in Materials and Methods. Equal loading was confirmed by immunoblotting for actin.

constitutive induction of the AP1 complex might depend on a higher level of stress in AT9RM and in AT3RM cells, with respect to the control and AT44RM lines. This opinion is confirmed when the expression of metallothioneins is evaluated. These molecules are classical stress response proteins, belonging to the anti-oxidant cellular system. The transcription of the two ubiquitous isoforms, MT1A and MT2A, appears upregulated in AT9RM cells and AT3RM, but not modulated in AT44RM cells.

We do not ignore that these data on the transcription of a limited number of genes need to be completed and integrated by a wider analysis using an improved approach based on the DNA-microarrays.

When on the same genes we evaluated the protein levels by immunoblotting, the results confirm those recorded on the mRNA transcripts. Regarding the metallothioneins we measured an increase of the protein levels in AT3RM and AT9RM cells, while no significant differences are detected in AT44RM with respect to the control (Fig. 8). According to the transcriptional data, no significant changes in p53 and c-myc proteins occur in AT cells with respect to the control (data not shown). This is also in accordance to what reported by other authors for p53 in AT9RM cells [Gatei et al., 2001]. Therefore, from these data we can infer a good correlation in AT cells between the changes at the transcriptional level and those at the protein levels.

DISCUSSION

The hypothesis supporting our work is that rearrangements in chromatin structure and organization should occur in cells with *ATM* mutations and determine alterations in the transcription of important genes. These events occurring down-stream of the genetic lesions, in our opinion, should support the variability observed at the level of clinical phenotype and disease severity in AT patients. In a previous report these differences were put in relationship with the level of the ATM damage [Stewart et al., 2001]. Patients with milder forms of AT syndrome still produce modest amounts of protein, whereas more severe forms present truncated or unstable proteins. However, no direct correlation between the level of ATM protein and the cell radiosensitivity, a classical symptom of AT syndrome, has still been proven [Gilad et al., 1998]. On the contrary, a coupling between radiosensitivity and chromatin decondensation has been described [Djuzenova and Flentje, 2001].

Our hypothesis started from these considerations and proposed that, more in general, rearrangements of chromatin structure might represent one of the effects of the *ATM* mutations, with down-stream relapses on the transcription profile and phenotype of the cells.

AT9RM are an "AT variant" with the features of the milder form of AT syndrome, such as reduced radiosensitivity and intermediate clinical symptoms [Chessa et al., 1992]. According to that, in this cell-line the ATM protein is still detectable, even if its level is lower than 20% and it is less stable than the normal protein [Gilad et al., 1998]. This could depend on the C-T substitution in the FATC domain, which would cause a shortening of the protein and a reduction of the biochemical activity [Lavin et al., 2004]. In accordance with the lower radiosensitivity, AT9RM cells show an increase of the average chromatin condensation and a reorganization of the chromatin domains with respect to the control. The low severity of the AT syndrome in this cell-line finds confirmation on the unmodified transcription of two proapoptotic genes, p53 and p21, which respond to DNA damage. Moreover, AT9RM present a slight upregulation of the three oncogenes and metallothionein 2A, which may suggest a stress condition for these cells. Since the protective role of ATM kinase against free radicals [Rotman and Shiloh, 1997], its defects may increase the oxidative stress of the cells and induce the expression of MTs and c-fos in the attempt of reducing it [Bakka et al., 1981; Satoh et al., 1994].

The second cell-line under analysis, the AT3RM, exhibits a chromatin remodeling opposite to that observed in AT9RM. An average chromatin decondensation occurs together with the enlargement of the nucleus and the disappearance of the highly condensed domains. These results are in accordance with the increased radiosensitivity previously reported for this cell-line. Moreover the lack of ATM protein measured by immunoblot could explain the observed downregulation of p53 and p21. Since ATM is directly involved in p53 activation [Kastan et al., 1992], the lack of this kinase should produce, in fact, the accumulation of the inactive forms of p53, which in turn would act as a negative feedback on its transcription. Functional inactivation of p53 protein renders the cells more susceptible to oncogenic stimuli and environmental insults [Ko and Prives, 1996; Giaccia and Kastan, 1998; North and Hainaut, 2000], higher risk of tumor formation, and neurodegeneration [Westphal et al., 1997; Xu et al., 1998; Nilsson and Cleveland, 2003]. In accordance to that, the oncogenes c-myc, c-fos, and c-jun, which are usually coupled with the neoplastic transformation, are upregulated. Also metallothioneins are induced in AT3RM, suggesting this cell-line is more stressed, already in physiological conditions, than the control.

The third cell-line under analysis, AT44RM, exhibits only a slight increase of chromatin condensation with respect to the control. In accordance to that, the nucleus of these cells preserves a 3D organization rather similar to the healthy cells. A marked downregulation of the three oncogenes under analysis, c-myc, c-jun, and c-fos, occurs in this cell-line, together with a fainter inhibition of metallothionein transcription, MT2A in particular. These three oncogenes are involved in the regulation of cell-cycle progression and apoptosis induction, therefore their reduced transcription should mean that AT44RM do not activate the mechanisms of cell-cycle block because the mutation does not damage seriously the cell function. Similar considerations can be done regarding the MT downregulation.

By resuming, the results of our work suggest that AT3RM is the most altered cell-line both at the level of nuclear architecture and chromatin organization. At the opposite side AT44RM line seems apparently poorly altered with respect to control. These structural changes could depend on major malfunctioning of the DSBs repair system, which lies under the control of ATM protein. These data are in accordance with previous reports indicating as the chromatin organization of AT cells is rather similar to that of stressed cells [Hittelman and Pandita, 1994].

We can conclude that in AT3RM the ATM mutation is rather severe and causes the complete lack of the protein and a marked chromatin remodeling affecting significantly the expression of all the genes under analysis. On the contrary, in AT9RM cells the presence of ATM protein, even if at lower levels, produces an increase of chromatin condensation which alters only the transcription and expression of the three oncogenes and metallothioneins, whereas p21 and p53 expression are unmodified. At last AT44RM cells, which preserve a nuclear organization rather similar to the control, do not exhibit upregulated genes and this suggests a low severe disease severity.

It remains to clarify if the structural changes we observed in chromatin organization depend directly on the ATM through its association with the nuclear matrix [Gately et al., 1998] and euchromatin [Scherthan et al., 2000], or if ATM kinases regulates the activity of remodeling factors acting down-stream [Koundrioukoff et al., 2004].

ACKNOWLEDGMENTS

REFERENCES

Abraham RT. 2001. Cell-cycle checkpoint signaling through the ATM and ATR kinases. Genes Dev 15: 2177–2196.

Agard DA. 1984. Optical sectioning microscopy: Cellular architecture in three dimensions. Annu Rev Biophys Bioeng 13:191–219.

Agard DA, Hiraoka Y, Shaw P, Sedat JW. 1989. Fluorescence microscopy in three dimensions. Meth Cell Biol 30:353–377.

Allegra P, Sterner R, Clayton DF, Allfrey VG. 1987. Affinity chromatographic purification of nucleosomes containing transcriptionally active DNA sequences. J Mol Biol 196: 379–388.

Allera C, Lazzarini G, Patrone E, Alberti I, Barboro P, Sanna P, Merchiori A, Parodi S, Balbi C. 1997. The condensation of chromatin in apoptotic thymocytes shows a specific structural change. J Biol Chem 272:10817–10822.

Allfrey VG, Chen TA. 1991. Nucleosomes of transcriptionally active chromatin: Isolation of template-active nucleosomes by affinity chromatography. Meth Cell Biol 55: 315–333.

Bakka A, Endresen L, Johnsen AB, Edminson PD, Rugstad HE. 1981. Resistance against cis-dichlorodiammineplatinum in cultured cells with a high content of metallothionein. Toxicol Appl Pharmacol 61:215–226.

Bakkenist CJ, Kastan MB. 2003. DNA damage activates ATM through intermolecular autophosphorylation and dimer dissociation. Nature 421:499–506.

Balbi C, Abelmoschi ML, Gogioso L, Parodi S, Barboro P, Cavazza B, Patrone E. 1989. Structural domains and conformational changes in nuclear chromatin: A quantitative thermodynamic approach by differential scanning calorimetry. Biochemistry 28:3220–3227.

Bartels PH. 1979. Numerical evaluation of cytological data. Description of profiles. Anal Quant Cytol Histol 1:20–28.

Beattie JH, Owen HL, Wallace SM, Arthur JR, Kwun IS, Hawksworth GM, Wallace HM. 2005. Metallothionein overexpression and resistance to toxic stress. Toxicol Lett 157:69–78.

Belmont AS, Bruce K. 1994. Visualization of G1 chromosomes: A folded, twisted, supercoiled chromonema model of interphase chromatid structure. J Cell Biol 127:287–302.

Belmont A, Kendall FM, Nicolini C. 1980. Coupling of nuclear morphometry to cell geometry and growth in human fibroblasts. Cell Biophys 2:165–175.

Belmont A, Kendall FM, Nicolini C. 1984. Three-dimensional intranuclear DNA organization in situ: Three states of condensation and their redistribution as a function of nuclear size near the G1-S border in HeLa S-3 cells. J Cell Sci 65:123–138.

Belmont A, Dietzel S, Nye A, Strukov Y, Tumbar T. 1999. Large scale chromatin structure and function. Curr Opin Cell Biol 11:307–311.

Bianchi A, Becuwe P, Collet P, Keller JM, Domenjoud L, Dauca M. 2002. Clofibric acid downregulation of metallothionein IIA in HepG2 human hepatoma cells. Biochem Pharmacol 63:237–245.

Boulaire J, Fotedar A, Fotedar R. 2000. The functions of the cdk-cyclin kinase inhibitor p21WAF1. Pathol Biol 48: 190–202.

Bradford MM, 1976. A rapid and sensitive method for the quantitation of microgram quantities of protein utilizing the principle of protein-dye binding. Anal Biochem 72: 248–254.

Bubulya PA, Spector DL. 2004. "On the move"ments of nuclear components in living cells. Exp Cell Res 296: 4–11.

Chessa L, Petrinelli P, Antonelli A, Fiorilli M, Elli R, Marcucci L, Federico A, Gandini E. 1992. Heterogeneity in ataxia-telangiectasia: Classical phenotype associated with intermediate cellular radiosensitivity. Am J Med Genet 42:741–746.

Chessa L, Lisa A, Fiorani O, Zei G. 1994. Ataxia telangiectasia in Italy: Genetic analysis. Int J Rad Biol 66:S31–S33.

Chomczynski P, Sacchi N. 1987. Single-step method of RNA isolation by acid guanidinium thiocyanate-phenol-chloroform extraction. Anal Biochem 162:156–159.

Concannon P, Gatti RA. 1997. Diversity of ATM gene mutations detected in patients with ataxia-telangiectasia. Hum Mutat 10:100–107.

Cosma MP, Tanaka T, Nasmyth K. 1999. Ordered recruitment of transcription and chromatin remodeling factors to a cell cycle- and developmentally regulated promoter. Cell 97:299–311.

Cremer T, Cremer C. 2001. Chromosome territories, nuclear architecture and gene regulation in mammalian cells. Nature Rev Gen 2:292–301.

Cremer M, Kupper K, Wagler B, Wizelman L, Von Hase J, Weiland Y, et al. 2003. Inheritance of gene density-related higher order chromatin arrangements in normal and tumor cell nuclei. J Cell Biol 162:809–820.

Djuzenova CS, Flentje M. 2001. Light scatter and DNA accessibility to propidium iodide of ataxia telangiectasia and fanconi anemia cells. Biochem Biophys Res Commun 286:365–371.

Ehrenhofer-Murray AE. 2004. Chromatin dynamics at DNA replication, transcription and repair. Eur J Biochem 271: 2335–2349.

Gatei M, Shkedy D, Khanna KK, Uziel T, Shiloh Y, Pandita TK, Lavin MF, Rotman G. 2001. Ataxia-telangiectasia: Chronic activation of damage-responsive functions is reduced by α-lipoic acid. Oncogene 20:289–294.

Gately DP, Hittle JC, Chan GK, Yen TJ. 1998. Characterization of ATM expression, localization, and associated DNA-dependent protein kinase activity. Mol Biol Cell 9: 2361–2374.

Gavazzo P, Vergani L, Mascetti GC, Nicolini C. 1997. Effects of histone acetylation on chromatin structure. J Cell Biochem 64:466–475.

Giaccia AJ, Kastan MB. 1998. The complexity of p53 modulation: Emerging patterns from divergent signals. Genes Dev 12:2973–2983.

Gilad S, Khosravi R, Shkedy D, Uziel T, Ziv Y, Savitsky K, Rotman G, Smith S, Chessa L, Jorgensen TJ, Harnik R, Frydman M, Sanal O, Portnoi S, Goldwicz Z, Jaspers NG, Gatti RA, Lenoir G, Lavin MF, Tatsumi K, Wegner RD, Shiloh Y, Bar-Shira A. 1996. Predominance of null mutations in ataxia-telangiectasia. Hum Mol Genet 5:433–439.

Gilad S, Chessa L, Khosravi R, Russell P, Galanty Y, Piane M, Gatti RA, Jorgensen TJ, Shiloh Y, Bar-Shira A. 1998. Genotype–phenotype relationships in ataxia-telangiectasia and variants. Am J Hum Genet 62:551–561.

Goodarzi AA, Lees-Miller SP. 2004. Biochemical characterization of the ataxia-telangiectasia mutated (ATM) protein from human cells. DNA Repair 3:753–767.

Grattarola M, Spaggiari S, Chessa L, Savio C, Nicolini C, Vergani L. 2003. A structural characterization of in situ chromatin on cell-lines isolated from patients affected by ataxia telangiectasia. Int J Biol Macromol 33: 23–29.

Guo CY, Wang Y, Brautigan DL, Larner JM. 1999. Histone H1 dephosphorylation is mediated through a radiation-induced signal transduction pathway dependent on ATM. J Biol Chem 26:18715–18720.

Gupta A, Sharma GG, Young CS, Agarwal M, Smith ER, Paull TT, Lucchesi JC, Khanna KK, Ludwig T, Pandita TK. 2005. Involvement of human MOF in ATM function. Mol Cell Biol 25:5292–5305.

Haussinger D. 1996. The role of cellular hydration in the regulation of cell function. Biochem J 31:697–710.

Hiraoka Y, Sedat JW, Agard DA. 1987. The use of a charge-coupled device for quantitative optical microscopy of biological structures. Science 238:36–41.

Hittelman WN, Pandita TK. 1994. Possible role of chromatin alteration in the radiosensitivity of ataxia-telangiectasia. Int J Radiat Biol 66:S109–S113.

Kastan MB, Zhan Q, el-Deiry WS, Carrier F, Jacks T, Walsh WV, Plunkett BS, Vogelstein B, Fornace AJ, Jr. 1992. A mammalian cell cycle checkpoint pathway utilizing p53 and GADD45 is defective in ataxia-telangiectasia. Cell 7:587–597.

Ko LJ, Prives C. 1996. p53: Puzzle and paradigm. Genes Dev 10:1054–1072.

Koundrioukoff S, Polo S, Almouzni G. 2004. Interplay between chromatin and cell cycle checkpoints in the context of ATR/ATM-dependent checkpoints. DNA Repair 3:969–978.

Kurz EU, Lees-Miller SP. 2004. DNA damage-induced activation of ATM and ATM-dependent signaling pathways. DNA Repair 3:889–900.

Lachner M, O'Sullivan RJ, Jenuwein T. 2003. An epigenetic road map for histone lysine methylation. J Cell Sci 116:2117–2124.

Laemmli UK. 1970. Cleavage of structural proteins during the assembly of the head of bacteriophage T4. Nature 227:680–685.

Lavin MF, Scott S, Gueven N, Kozlov S, Peng C, Chen P. 2004. Functional consequences of sequence alterations in the ATM gene. DNA Repair 3:1197–1205.

Lim DS, Kirsch DG, Canman CE, Ahn JH, Ziv Y, Newman LS, Darnell RB, Shiloh Y, Kastan MB. 1998. ATM binds to beta-adaptin in cytoplasmic vesicles. Proc Natl Acad Sci USA 95:10146–10151.

Marchi B, Burlando B, Panfili I, Pondero F, Viarengo A, Gallo G, 2005. Heavy metal interference with growth hormone signalling in trout hepatoma cells RTH-149. Biometals 18:179–190.

Marmorstein R. 2001. Structure and function of histone acetyltransferases. Cell Mol Life Sci 58:693–703.

Marshall WF. 2003. Gene expression and nuclear architecture during development and differentiation. Mech Dev 120:1217–1230.

Mascetti G, Vergani L, Diaspro A, Carrara S, Radicchi G, Nicolini C. 1996. Effect of fixatives on calf thymocytes chromatin as analyzed by 3D high-resolution fluorescence microscopy. Cytometry 23:110–119.

Mascetti G, Carrara S, Vergani L. 2001. The relationship between fiber folding and dye uptake for in situ chromatin stained with a DNA-selective dye. Cytometry 44:113–119.

Nicolini C, Vergani L, Diaspro A, Scelza P. 1988a. Native chromatin and damage induced by nuclease. Biochem Biophys Res Commun 155:1396–1403.

Nicolini C, Diaspro A, Vergani L, Cittadini G. 1988b. In situ thermodynamics characterization of chromatin and other macromolecules during the cell cycle. Int J Biol Macrom 10:137–144.

Nigg EA, Blangy A, Lane HA. 1996. Dynamic changes in nuclear architecture during mitosis: On the role of protein phosphorylation in spindle assembly and chromosome segregation. Exp Cell Res 22:174–180.

Nilsson JA, Cleveland JL. 2003. Myc pathways provoking cell suicide and cancer. Oncogene 22:9007–9021.

North S, Hainaut P. 2000. p53 and cell-cycle control: A finger in every pie. Pathol Biol 48:255–270.

Nye AC, Rajendran RR, Stenoien DL, Mancini MA, Katzenellenbogen BS, Belmont AS. 2002. Alteration of large-scale chromatin structure by estrogen receptor. Mol Cell Biol 22:3437–3449.

Polach KJ, Widom J. 1995. Mechanism of protein access to specific DNA sequences in chromatin: A dynamic equilibrium model for gene regulation. J Mol Biol 254:130–149.

Rich T, Allen RL, Wyllie AH. 2000. Defying death after DNA damage. Nature 407:777–783.

Rotman G, Shiloh Y. 1997. The ATM gene and protein: Possible roles in genome surveillance, checkpoint controls and cellular defence against oxidative stress. Cancer Surv 29:285–304.

Rozen S, Skaletsky HJ. 2000. Primer3 on the WWW for general users and for biologist programmers. In: Krawetz S., Misener S, editors. Bioinformatics methods and protocols: Methods in molecular biology. Totowa, NJ: Humana Press, pp 365–386 (Code available at http://www-genome.wi.mit.edu/genome_software/other/primer3.html

Sandoval N, Platzer M, Rosenthal A, Dork T, Bendix R, Skawran B, Stuhrmann M, Wegner RD, Sperling K, Banin S, Shiloh Y, Baumer A, Bernthaler U, Sennefelder H, Brohm M, Weber BH, Schindler D. 1999. Characterization of ATM gene mutations in 66 ataxia telangiectasia families. Hum Mol Genet 8:69–79.

Satoh M, Cherian MG, Imura N, Shimizu H. 1994. Modulation of resistance to anticancer drugs by inhibition of metallothionein synthesis. Cancer Res 54:5255–5257.

Savitsky K, Bar-Shira A, Gilad S, Rotman G, Ziv Y, Vanagaite L, Tagle DA, Smith S, Uziel T, Sfez S, Ashkenazi M, Pecker I, Frydman M, Harnik R, Sankhavaram RP, Simmons A, Clines GA, Sartiel A, Gatti RA, Chessa L, Sanal O, Lavin MF, Jaspers NGJ, Taylor AMR, Arlett CF, Miki T, Weissman SM, Lovett M, Collins FS, Shiloh Y. 1995a. A single ataxia telangiectasia gene with a product similar to PI-3 kinase. Science 268:1749–1753.

Savitsky K, Sfez S, Tagle DA, Ziv Y, Sartiel A, Collins FS, Shiloh Y, Rotman G. 1995b. The complete sequence of the coding region of the ATM gene reveals similarity to cell cycle regulators in different species. Hum Mol Genet 4:2025–2032.

Scherthan H, Jerratsch M, Dhar S, Wang YA, Goff SP, Pandita TK. 2000. Meiotic telomere distribution and Sertoli cell nuclear architecture are altered in Atm- and Atm-p53-deficient mice. Mol Cell Biol 20:7773–7783.

Schonherr E, Levkau B, Schaefer L, Kresse H, Walsh K. 2001. Decorin-mediated signal transduction in endothelial cells. Involvement of Akt/protein kinase B in upregulation of p21(WAF1/CIP1) but not p27(KIP1). J Biol Chem 276:40687–40692.

Shaulian E, Karin M. 2002. AP-1 as a regulator of cell life and death. Nat Cell Biol 4:131–136.

Shiloh Y. 2003. ATM and related protein kinases: Safeguarding genome integrity. Nature Rew Cancer 3:155–168.

Shiloh Y, Kastan MB. 2001. ATM: Genome stability, neuronal development, and cancer cross paths. Adv Cancer Res 83:209–254.

Smilenov LB, Dhar S, Pandita TK. 1999. Altered telomere nuclear matrix interactions and nucleosomal periodicity

in ataxia telangiectasia cells before and after ionizing radiation treatment. Mol Cell Biol 19:6963–6971.

Stein GS, van Wijnen AJ, Stein JL, Lian JB, Pockwinse SH, McNeil S. 1999. Implications for interrelationships between nuclear architecture and control of gene expression under microgravity conditions. FASEB J 13:157–166.

Stewart GS, Last JI, Stankovic T, Haites N, Kidd AM, Byrd PJ, Taylor AM. 2001. Residual ataxia telangiectasia mutated protein function in cells from ataxia telangiectasia patients, with 5762ins137 and 7271T → G mutations, showing a less severe phenotype. J Biol Chem 276:30133–30141.

Touchette NA, Cole RD. 1985. Differential scanning calorimetry of nuclei reveals the loss of major structural features in chromatin by brief nuclease treatment. Proc Natl Acad Sci USA 82:2642–2645.

van Gent DC, Hoeijmakers JH, Kanaar R. 2001. Chromosomal stability and the DNA double-stranded break connection. Nat Rev Genet 2:196–206.

Vergani L, Gavazzo P, Mascetti G, Nicolini C. 1994. Ethidium bromide intercalation and chromatin structure: A spectropolarimetric analysis. Biochemistry 33:6578–6585.

Vergani L, Mascetti G, Nicolini C. 1998. Effects of polyamines on higher-order folding of in situ chromatin. Mol Biol Rep 25:237–244.

Vergani L, Fugazza G, Chessa L, Nicolini C. 1999. Changes of chromatin condensation in one patient with ataxia telangiectasia disorder: A structural study. J Cell Biochem 75:578–586.

Vergani L, Grattarola M, Nicolini C. 2004. Modifications of chromatin structure and gene expression following

induced alterations of cellular shape. Int J Biochem Cell Biol 36:1447–1461.

Vogelstein B, Kinzler KW. 2004. Cancer genes and the pathways they control. Nat Med 10:789–799.

Walker J, Chen TA, Sterner R, Berger M, Winston F, Allfrey VG. 1990. Affinity chromatography of mammalian and yeast nucleosomes. Two modes of binding of transcriptionally active mammalian nucleosomes to organomercurial-agarose columns, and contrasting behavior of the active nucleosomes of yeast. J Biol Chem 265:5736–5746.

Weizman N, Shiloh Y, Barzilai A. 2003. Contribution of the Atm protein to maintaining cellular homeostasis evidenced by continuous activation of the AP-1 pathway in Atm-deficient brains. J Biol Chem 278:6741–6747.

Westphal CH, Rowan S, Schmaltz C, Elson A, Fisher DE, Leder P. 1997. atm and p53 cooperate in apoptosis and suppression of tumorigenesis, but not in resistance to acute radiation toxicity. Nat Genet 16:397–401.

Workman JL, Kingston RE. 1998. Alteration of nucleosome structure as a mechanism of transcriptional regulation. Annu Rev Biochem 67:545–579.

Xu Y, Ashley T, Brainerd EE, Bronson RT, Meyn MS, Baltimore D. 1996. Targeted disruption of ATM leads to growth retardation, chromosomal fragmentation during meiosis, immune defects, and thymic lymphoma. Genes Dev 10:2411–2422.

Xu Y, Yang EM, Brugarolas J, Jacks T, Baltimore D. 1998. Involvement of p53 and p21 in cellular defects and tumorigenesis in Atm−/− mice. Mol Cell Biol 18:4385–4390.

Zink D, Fischer AH, Nickerson JA. 2004. Nuclear structure in cancer cells. Nat Rev Cancer 4:677–687.